

# Estimation of the FR4 Microwave Dielectric Properties at Cryogenic Temperature for Quantum-Chip-Interface PCBs Design

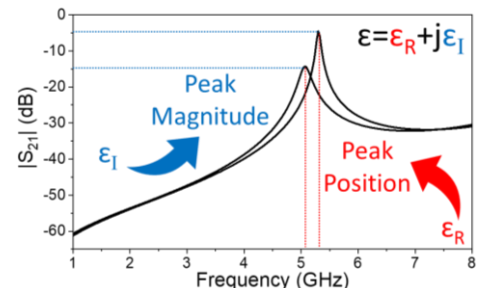
A. Paghi<sup>1</sup>, G. Trupiano<sup>1</sup>, C. Puglia<sup>1,2</sup>, H. Burgaud<sup>1,3</sup>, G. De Simoni<sup>1</sup>, A. Greco<sup>1</sup>, and F. Giazotto<sup>1</sup>

<sup>1</sup> Istituto Nanoscienze-CNR and Scuola Normale Superiore, Piazza San Silvestro 12, 56127 Pisa, Italy.

<sup>2</sup> INFN Sezione di Pisa, Largo Bruno Pontecorvo 3, I-56127 Pisa, Italy.

<sup>3</sup> Ecole Normale Supérieure, 45 rue d'Ulm, 75005 Paris, France.

**Abstract** — Ad-hoc interface PCBs are today the standard connection between cryogenic cabling and quantum chips. Besides low-loss and low-temperature-dependent-dielectric-permittivity materials, FR4 provides a low-cost solution for fabrication of cryogenic PCBs. Here, we report on an effective way to evaluate the dielectric performance of a FR4 laminate used as substrate for cryogenic microwave PCBs. We designed a coplanar waveguide  $\lambda/2$  open-circuit series resonator and we fabricated the PCB using a low-cost manufacturing process. Such a geometry allows to exploit the resonance peak of the resonator to measure the variation of the complex dielectric permittivity as a function of the temperature. Resonance peak frequency and magnitude were used as sensing parameters for the real part of dielectric permittivity and dielectric loss tangent, respectively. We estimated a 9 % reduction of the real part of the dielectric permittivity and a 70 % reduction of the dielectric loss tangent in the temperature range from 300 to 4 K. The proposed approach can be immediately extended to the detection of cryogenic temperature-dependent dielectric performance of any kind on substrate.



**Keywords** — cryogenic, dielectric permittivity, FR4, loss tangent, quantum, temperature.

## I. INTRODUCTION

In the last years, physicists and engineers focused on the development of new materials, devices, and technologies for quantum nanoelectronics [1][2]. Future useful quantum architectures will likely require the readout, manipulation, and interaction of several on-chip quantum bits, nanoelectronic devices, and control systems [3][4]. As achieved in today's integrated circuits, it is reasonable to assume that future intra- and inter-connections in quantum architectures could be achieved by lithographically defined traces, removing the limit to directly address each individual quantum component from the outside. However, the current state of the art on quantum electronics requires the direct readout and manipulation of any aspect of the proposed device at cryogenic temperature, typically controlled by external measurement setups at room temperature [5][6]. Ad-hoc interface printed circuit boards (PCBs) provided with DC and RF connectors, are today the standard interface between cryogenic cabling and quantum chips, with application in cryogenic filtering, microwave sample holder, and bias tee PCBs [7][8]. Increasing the complexity of the quantum chips, more sophisticated interface PCBs with a higher number of electrical connections and components are required [5]. In this framework, low-loss and

low-temperature-dependent-dielectric-permittivity materials, such as Rogers<sup>TM</sup>, have been in a leading position in the developing of microwave and millimeter-wave frequency design of ad-hoc cryogenic PCBs, compared to standard substrates as FR4 [7][8]. Yet, manufacturing PCB prototypes with FR4 could be largely cheaper than the Rogers<sup>TM</sup> counterpart. It is known that the FR4 dielectric properties are temperature dependent and are not usually provided in the cryogenic temperature range by the manufacturers [9]. Consequently, it is worth characterizing commercial FR4 laminates to estimate their dielectric properties to improve the PCB prototyping process at cryogenic temperatures. The dielectric resonator method is typically used for the microwave characterization of materials, using Hakki-Coleman dielectric resonators [10][11], single post dielectric resonators [12], and split post dielectric resonators [12][13][14][15]. However, these techniques require highly specialized measurement setups to perform the dielectric characterization.

Here, we report on an effective way to evaluate the dielectric performance of a FR4 laminate used as substrate for cryogenic microwave PCBs. We designed a ground-backed coplanar waveguide (GB-CPW)  $\lambda/2$  open-circuit series resonator and we fabricated the PCB using a low-cost commercially available manufacturing process. Such a geometry allows us to

exploit the resonance peak of the resonator to measure the variation of the complex dielectric permittivity as a function of the temperature. The manufacturing capabilities enable the fabrication of 100 mm to several cm in-plane geometric features with maximum variations of 50-100 mm compared to the PCB design. We estimated a 9 % reduction of the real part of the dielectric permittivity and a 70 % reduction of the dielectric loss tangent in the temperature range from 300 to 4 K, which should be considered in the cryogenic PCB design.

## II. MATERIALS AND METHODS

### A. PCB Design, Simulation, and Fabrication

The PCB was designed with KiCAD (v5.1.7) using front and bottom copper (Cu) level and simulated with Sonnet (v18.56, cell size of 25 mm, ABS sweep from 300 kHz to 8.5 GHz). PCBs were manufactured exploiting the PCBWay [16] Normal process. FR-4 (Kingboard Laminates Holdings Ltd., laminate KB-6165F, prepreg KB-6065F, 1.6 mm thickness, 150 °C glass transition temperature) was used as dielectric substrate for the PCB, with Cu layers on the top and bottom with a minimum track/spacing of 127 mm and minimum vias hole size of 300 mm (tenting vias technology). 1 oz Cu was chosen as Cu finish and Electroless Nickel Immersion Gold (ENIG) as surface finish.

### B. Cryogenic Measurement System

SMA connectors (Amphenol RF, 901-10112) were soldered to the PCBs and used to test the RF electrical behavior of the system. PCBs were provided with an ad-hoc manufactured back Cu (Cu-ETP CW004A EN 13601) thermal plate and covered with an ad-hoc aluminum (Al) top faraday cage (38 mm × 10 mm × 3 mm) to avoid unwanted resonance frequencies induced by the cm-size cavity created by the 40 K Cu cylindrical shield (Figure 1a, green dashed line) of the closed cycle cryocooler (Advanced Research System, DE-210) we used to perform the temperature characterization of the device (Figure 1b). PCBs were mounted in contact with the 4 K cold head (Figure 1a, red solid line) and connected with coaxial SMA cables (Fairview Microwave, FMC0202085, Figure 1a, blue solid line). Power attenuators (Mini-Circuits, BW-S3-2W263+, 3 dB attenuation) were used to thermalize electronic temperatures both at 40 K and 4 K. We performed temperature sweeps from 4 K to 300 K at a chamber residual pressure of 7E-6 mbar, measuring the scattering parameters in the frequency range from 300 kHz to 8.5 GHz (1.7 MHz step, 0 dBm input power) using a Vectorial Network Analyzer (VNA, Pico Technology, PicoVNA 108). The calibration of the VNA was performed with the short, open, load, and through procedure (SOLT, Pico Technology, Standard SOLT female SMA cal-kit). At 300 K, we measured all the two-port S-parameter magnitudes ( $|S_{11}|$ ,  $|S_{21}|$ ,  $|S_{12}|$ , and  $|S_{22}|$ ) by putting the reference planes prior the PCB SMA connectors (*method 1*). On the other hand, for the on-cryostat measurements, we collected only the  $|S_{21}|$  spectra by moving the reference planes at the input of the cryostat (Figure 1a, black dashed lines, *method 2*). By doing this, temperature-dependent  $|S_{21}|$  also includes the electrical performance of cables and power attenuators used to connect the PCB from the internal to the external of the cryostat ( $|S_{21}|_{\text{PCB+Sys}}$ ). To extrapolate the PCB

$|S_{21}|$  itself ( $|S_{21}|_{\text{PCB}}$ ), we took the temperature dependent  $|S_{21}|$  of a reference through (Figure S1) positioned in place of the PCB ( $|S_{21}|_{\text{Sys}}$ ). We extrapolated the  $|S_{21}|_{\text{PCB}}$  by the following equation:  $S_{21}|_{\text{PCB}} = |S_{21}|_{\text{PCB+Sys}} - |S_{21}|_{\text{Sys}}$ .

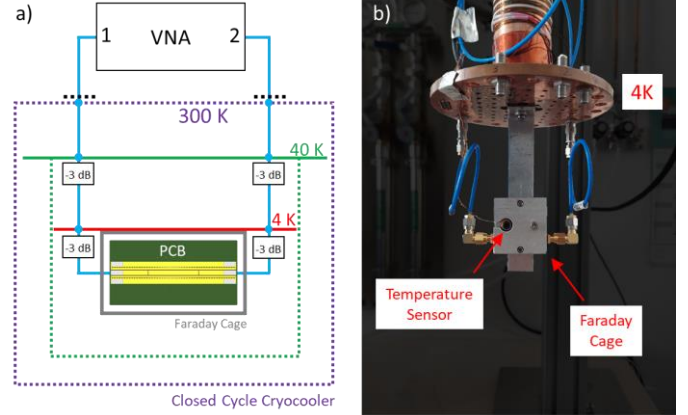


Fig. 1. The microwave cryogenic setup implemented. a) Schematic diagram of the measurement setup. Violet, green, and red dashed and solid lines are used to identify thermal shields and plates, respectively. Blue solid lines identify electrical cables. Black dashed lines identify the VNA reference planes. b) Picture of the PCB mounted on the 4K cold head and connected to the VNA using coaxial SMA cables, highlighting the ad-hoc faraday cage manufactured and the position of the temperature sensor we used.

## III. RESULTS AND DISCUSSION

### A. PCB Design

Figure 2 shows the CAD of the manufactured PCB.

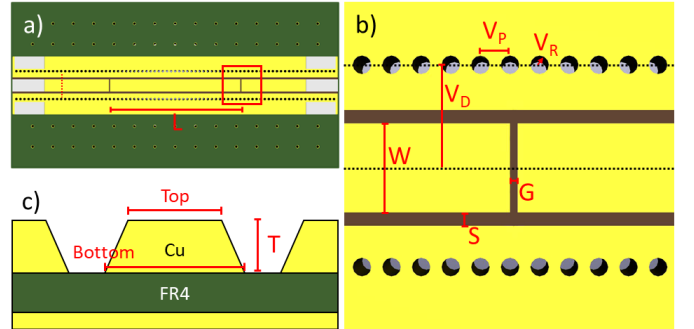


Fig. 2. CAD of the manufactured PCB. a) Overall top view of the PCB exhibiting the 5 GHz resonator and CPW. b) Zoom of the resonator capacitive coupling area in red square of a) showing the coupling gap, the signal line-ground plane spacing, and ground vias. c) In-section view of the red dashed lines in a) exhibiting bottom and top Cu thicknesses.

We designed a GB-CPW  $\lambda/2$  open-circuit series resonator (Figure 2) employing length ( $L$ ) of 16 mm and width ( $W$ ) of 1.5 mm connected with a GB-CPW by the two coupling capacitors, one for each side, exploiting a gap ( $G$ ) of 125 mm. We matched the impedance of the CPW and the resonator to  $Z_0 = 50 \Omega$  with a signal-line-ground separation ( $S$ ) of 225 mm. Higher order resonance modes suppression was obtained with ground vias placing ( $V_D = 1.6 \text{ mm} < \lambda_{\text{MAX}}/4$ ,  $V_P = 0.6 \text{ mm} < \lambda_{\text{MAX}}/4$ ,  $V_R = 0.3 \text{ mm}$ , with  $\lambda_{\text{MAX}} = c/(f_{\text{MAX}} \times \epsilon_{\text{R FR4}})$ ,  $c = 3 \times 10^8 \text{ m/s}$ ,  $f_{\text{MAX}} = 8.5 \text{ GHz}$ ,  $\epsilon_{\text{R FR4}} = 4.6$ ) [17]. Figure 2c shows the in-section view of the PCB depicting the typical Cu layer trapezoidal profile obtained via Cu acidic wet etching

involved in trace definition manufacturing step. The trapezoidal profile allows to define each in-plane geometry both on top and on bottom of the Cu trace.

### B. Morphological Characterization of the Manufactured PCB

Figure 3a shows a typical scanning electron microscopy (SEM, Zeiss, Merlin Gemini, 5 kV acceleration voltage, 30× magnification, 34° tilt, secondary electron detector) image of the coupling gap depicted in Figure 2b. The micrograph shows that the PCBWay Normal Process involved in the PCB manufacturing allows to achieve in-plane features in the range from 100 μm to several cm. A clear separation of the Cu traces (dark grey area) is observed from the FR4 substrate left exposed on the bottom side (light grey area). Cu traces are about 43 μm thick (Figure 3b) (Bruker, DektacXT, stylus radius 12.5 mm, force 3 mg).

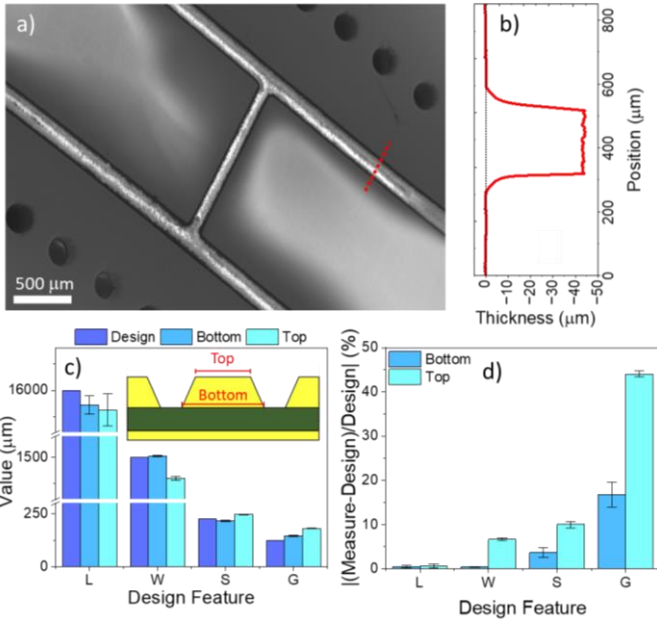


Fig. 3. Morphological characterization of the manufactured PCB. a) SEM image of the coupling gap area. b) Stylus profilometer analysis performed in the red dashed line of a) showing Cu trace thickness. c) Designed and measured top and bottom values of in-plane PCB geometries. The inset depicts the in-section PCB view. d) Absolute normalized relative variation of measured vs. designed in-plane PCB geometries. Data in c,d) are reported as the average value measured over  $n = 3$  PCBs, with error bars representing the standard deviation.

Figure 3c shows the comparison between the design parameters (dark blue) and top/bottom measured dimensions (light blue). We measured a maximum variation of about 100 mm in the case of L (bottom) value, compared to the design of 16 mm. Regarding G, we found that the fabrication process led to a top maximum value of 55 mm larger than the designed (125 mm). Figure 3d displays the absolute normalized relative variations (ANRV), defined as  $|\text{Measured value} - \text{Design value}|/\text{Design value}$ , for both top and bottom in-plane measured geometries. These results point out that for smaller features the fabrication error leads to larger ANRV. Specifically, we found a maximum 44 % variation for G (top), the smallest feature of the PCB. Such values are usually better

than the in-plane fabrication tolerance of  $\geq 20\%$  reported for the PCBWay Normal process.

### C. Microwave Electrical Behavior of the PCB at 300 K

Figure 4 shows typical measured and simulated S-parameters of the PCB at the temperature of 300 K.

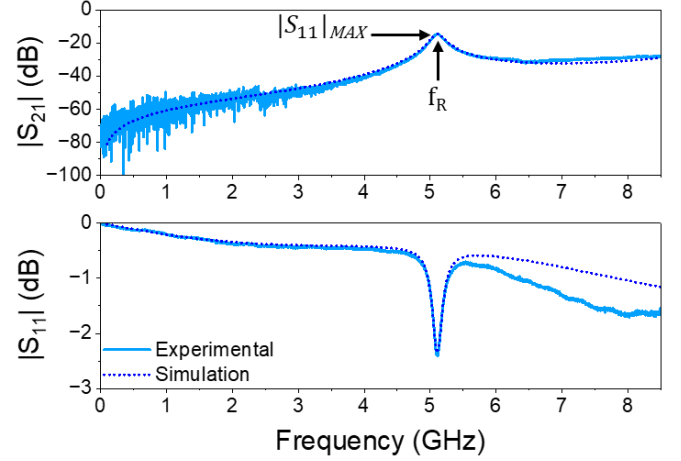


Fig. 4. Typical measured and simulated S-parameters of the PCB at 300 K.

A resonance peak (dip) is evident on  $|S_{21}|$  ( $|S_{11}|$ ) spectrum from which values of resonance frequency ( $f_R$ ) and  $|S_{21}|$  magnitude ( $|S_{21}|_{MAX}$ ) were extrapolated. We also calculated the quality factor ( $Q_{-10dB}$ ) as  $Q_{-10dB} = f_R/BW$ , where  $BW$  is the frequency bandwidth where the resonance peak value is reduced by -10 dB. We obtained values of  $f_R = 5.104 \pm 0.011$  GHz,  $|S_{21}|_{MAX} = -14.390 \pm 0.304$  dB, and  $Q_{-10dB} = 9.27 \pm 0.23$  (std evaluated with  $n = 3$  PCBs). We extrapolated the coefficient of variation ( $CV\% = 100 \times \text{average value} / \text{std}$ ) of  $f_R$ ,  $|S_{21}|_{MAX}$ , and  $Q_{-10dB}$ , which correspond respectively to 0.2%, 2% and 2.5%. We note that the CVs just calculated are very similar to the CVs of the geometrical features, hence 0.3% for L and 1.7% for G. This is not surprising since L and G are the geometrical features mostly affecting  $f_R$  and  $Q_{-10dB}$ , respectively.

The simulation was carried out with the design reported in Figure 2 using the measured parameters of Figure 3c. The parameters extracted from the simulation are the dielectric permittivity ( $\epsilon_R$ ) and the dielectric loss tangent ( $\tan\delta_e = \epsilon_1/\epsilon_R$ ). At 300 K, we extrapolated  $\epsilon_R = 4.80 \pm 0.04$  ( $n = 3$  PCBs), a value close to what reported by the PCB laminate manufacturer, namely 4.6 @ 1GHz. On the other hand, we retrieved  $\tan\delta_e = 0.033 \pm 0.003$  ( $n = 3$  PCBs), that is about two times higher than 0.016 @ 1 GHz reported as typical value. The last result could be related to the absence of SMA connectors on the performed simulations.

### D. Temperature-Dependent Microwave Electrical Behavior of the PCB

We then measured the temperature-dependent microwave electrical properties of the fabricated PCB with the measurement setup reported in Figure 1, extrapolating the dielectric properties vs. temperature behavior of the FR4 substrate chosen. We used  $f_R$  as sensing parameter for  $\epsilon_R$ ,

under the approximation of negligible changes of in-plane and out-of-plane PCB geometric features with the temperature [9]. At the same time,  $|S_{21}|_{\text{MAX}}$  was chosen as sensing parameter for both  $\tan\delta_e$  and  $\epsilon_1$ . Figure 5a shows the typical measured  $|S_{21}|$  spectra at different temperatures, from which both an increase of  $f_R$  and  $|S_{21}|_{\text{MAX}}$  are clearly observed.

Figure 5b shows the  $f_R$  vs. temperature trend; a monotonic increase of the resonance frequency from about 5.1 to 5.3 GHz was collected by decreasing the temperature. We extrapolated the  $\epsilon_R$  vs. temperature behavior employing the same simulation model previously described. We tuned the dielectric permittivity value in the simulation, we collected  $f_R$  in the simulated  $|S_{21}|$  spectra, and we fitted the  $f_R$  vs.  $\epsilon_R$  data with a linear curve ( $f_R = m \times \epsilon_R + q$ ), as shown in Figure S2a. The relationship was then used to extrapolate the  $\epsilon_R$  vs. temperature curve. Figure 5c shows values of the real part of the dielectric permittivity in the temperature range 4 K to 300 K, where a monotonic decrease from  $\epsilon_R = 4.82 \pm 0.05$  @ 300 K to  $\epsilon_R = 4.40 \pm 0.05$  @ 4 K is calculated ( $n = 3$  PCBs).

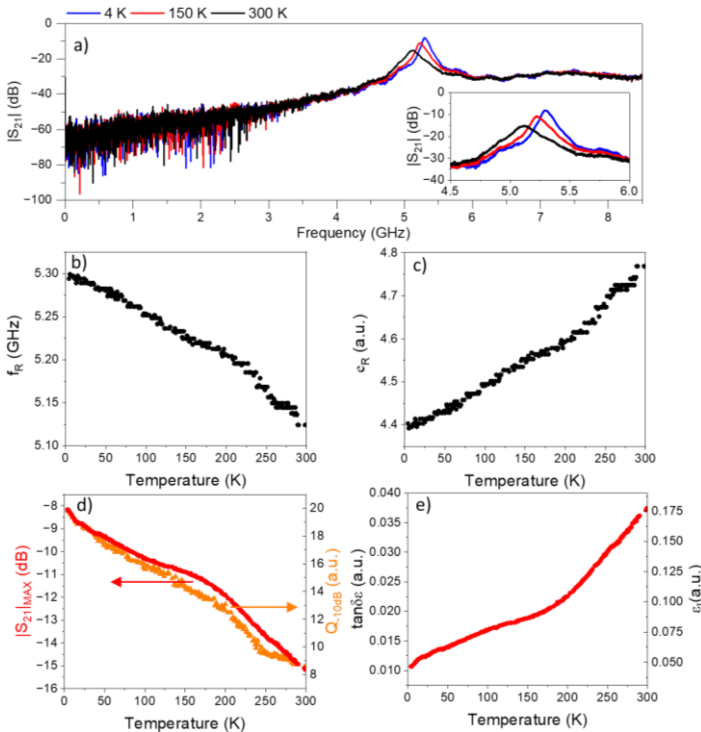


Fig. 5. Typical temperature-dependent microwave electrical behaviour of the PCB and FR4 laminate dielectric properties. a) Measured temperature-dependent  $|S_{21}|$  spectra. The inset shows the resonance peaks. b) Measured resonance frequency vs. temperature. c) Extrapolated real part of dielectric permittivity vs. temperature. d) (left) Measured  $|S_{21}|$  maximum and (right) quality factor vs. temperature. e) Extrapolated dielectric loss tangent and imaginary part of dielectric permittivity vs. temperature.

The  $|S_{21}|_{\text{MAX}}$  vs. temperature behavior is shown in Figure 5d. As reported for the resonance frequency, also in this case a monotonic increase of the maximum of the  $|S_{21}|$  spectrum from about -15.5 to -8 dB was observed by decreasing the temperature. We extrapolated the  $\tan\delta_e$  vs. temperature behavior, as well as the  $\epsilon_1$  vs. temperature trend, tuning the dielectric loss tangent value in the simulator, collecting  $|S_{21}|_{\text{MAX}}$  in the simulated  $|S_{21}|$  spectra, and fitting the  $|S_{21}|_{\text{MAX}}$

vs.  $\tan\delta_e$  data with a first order exponential decay curve ( $|S_{21}|_{\text{MAX}} = a_1 \times \exp(-\tan\delta_e / t_1) + q$ ), as shown in Figure S2b. The relationship was then used to extrapolate the  $\tan\delta_e$  vs. temperature ( $\epsilon_1$  vs. temperature) curve. Figure 5e shows both values of the dielectric loss tangent and the imaginary part of the dielectric permittivity in the temperature range 4 to 300 K, where a monotonic decrease from  $\tan\delta_e = 0.038 \pm 0.004$  @ 300 K to  $\tan\delta_e = 0.012 \pm 0.002$  @ 4 K is calculated ( $n = 3$  PCBs).

### E. Application to a Specific Case

Eventually, we focused on the simulation of the microwave performance of a cryogenic PCB embedding a GB-CPW at 4 K compared to 300 K (Figure 6a). CPWs are usually employed as communication links on quantum chips and interface PCBs to transmit microwave signals. The designed GB-CPW employs a length of 38 mm and a width of 1.5 mm. Signal-line-ground separations of 250 and 300 mm were used to match the characteristic impedance of the CPW to  $Z_0 = 50 \Omega$  at 4 and 300 K, respectively.

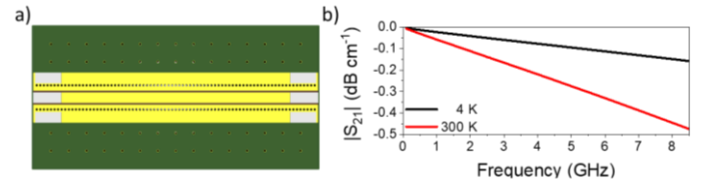


Fig. 6. Impact of the dielectric permittivity on the design of a cryogenic microwave PCB. a) CAD of an on-PCB GB-CPW. b) Simulated insertion losses of an on-PCB GB-CPW at 4 K and 300 K.

As shown in Figure 6b, a ~66 % reduction of the insertion losses ( $|S_{21}|$ , from  $-0.275 \text{ dB cm}^{-1}$  at 300 K to  $-0.095 \text{ dB cm}^{-1}$  at 4 K evaluated at 5 GHz) is achieved at 4 K compared to 300 K, which is related to the reduction of the dielectric loss tangent as the device temperature decreases.

We note that low-loss permittivity materials generally employed in cryogenic interface PCBs, like Rogers<sup>TM</sup>, present  $\tan\delta_e$  one order of magnitude lower than the FR4 estimated here [18]. Nonetheless, the usual selling price for the former is one order of magnitude higher than the latter. This fact imposes an important trade-off to take into account when engineering cryogenic PCBs.

## IV. CONCLUSION

In this work, we reported an effective procedure to evaluate the dielectric performance of a commercial FR4 dielectric laminate used as substrate for cryogenic microwave PCBs using a GB-CPW  $\lambda/2$  open-circuit series resonator. We fabricated the PCB using a low-cost manufacturing process, obtaining in-plane geometric features with maximum variations of 50-100  $\mu\text{m}$  compared to the PCB design. We used the resonance peak frequency and magnitude as sensing parameters for the real part of dielectric permittivity and dielectric loss tangent, estimating a reduction of about 9 and 70 % from 300 to 4 K, respectively. The temperature-dependent dielectric permittivity values were then used to design a cryogenic-specific FR4-based PCB embedding a

CPW. Such a cryogenic specific design showed a reduction of ~66 % of the insertion losses at 4 K, compared to the results achieved at 300 K.

[18] M. V. Jacob, J. Krupka, J. Mazierska, and M. Bialkowski, "Temperature dependence of complex permittivity of planar microwave materials," in *2006 Asia-Pacific Microwave Conference*, 2006, vol. 3, pp. 1453–1456.

## APPENDIX

### A. Error on $|S_{21}|$ spectra measurement

We used the  $|S_{21}|$  spectra measured at 300 K with *method 1* as gold standard for estimation of the microwave behavior of the PCB, since the reference planes of the VNA are directly placed at the input of the PCB SMA connectors with no spectra subtraction required. Compared to the spectra taken with *method 1*, at 300 K with *method 2* we estimated an error of ~-1 dB on  $|S_{21}|_{\text{MAX}}$ , while the error made on the evaluation of  $f_R$  is similar to the frequency sampling step. This leads to an error of ~14 % in estimation of  $\tan\delta_e$ .

## REFERENCES

- [1] F. Paolucci *et al.*, "Field-effect control of metallic superconducting systems," *AVS Quantum Sci.*, vol. 1, no. 1, Dec. 2019.
- [2] M. Colangelo *et al.*, "Large-Area Superconducting Nanowire Single-Photon Detectors for Operation at Wavelengths up to 7.4  $\mu\text{m}$ ," *Nano Lett.*, vol. 22, no. 14, pp. 5667–5673, Jul. 2022.
- [3] M. W. Johnson *et al.*, "A scalable control system for a superconducting adiabatic quantum optimization processor," *Supercond. Sci. Technol.*, vol. 23, no. 6, p. 065004, Jun. 2010.
- [4] D. Yohannes *et al.*, "High density fabrication process for single flux quantum circuits," *Appl. Phys. Lett.*, vol. 122, no. 21, May 2023.
- [5] S. Krinner *et al.*, "Engineering cryogenic setups for 100-qubit scale superconducting circuit systems," *EPJ Quantum Technol.*, vol. 6, no. 1, p. 2, Dec. 2019.
- [6] M. O. Tholén *et al.*, "Measurement and control of a superconducting quantum processor with a fully integrated radio-frequency system on a chip," *Rev. Sci. Instrum.*, vol. 93, no. 10, Oct. 2022.
- [7] J. I. Colless and D. J. Reilly, "Cryogenic high-frequency readout and control platform for spin qubits," *Rev. Sci. Instrum.*, vol. 83, no. 2, p. 023902, Feb. 2012.
- [8] J. I. Colless and D. J. Reilly, "Modular cryogenic interconnects for multi-qubit devices," *Rev. Sci. Instrum.*, vol. 85, no. 11, p. 114706, Nov. 2014.
- [9] P. Sagar *et al.*, "Investigation on Temperature Dependent Inductance (TDI) of a planar Multi-Layer Inductor (MLI) down to 4.2 K," *Rev. Sci. Instrum.*, vol. 91, no. 8, p. 085101, Aug. 2020.
- [10] M. V. Jacob, J. Mazierska, D. Ledenyov, and J. Krupka, "Microwave characterisation of CaF<sub>2</sub> at cryogenic temperatures using a dielectric resonator technique," *J. Eur. Ceram. Soc.*, vol. 23, no. 14, pp. 2617–2622, Jan. 2003.
- [11] S. Parida *et al.*, "Structural refinement, optical and microwave dielectric properties of BaZrO<sub>3</sub>," *Ceram. Int.*, vol. 38, no. 3, pp. 2129–2138, Apr. 2012.
- [12] J. Krupka and J. Mazierska, "Contactless Measurements of Resistivity of Semiconductor Wafers Employing Single-Post and Split-Post Dielectric-Resonator Techniques," *IEEE Trans. Instrum. Meas.*, vol. 56, no. 5, pp. 1839–1844, Oct. 2007.
- [13] J. Krupka, A. P. Gregory, O. C. Rochard, R. N. Clarke, B. Riddle, and J. Baker-Jarvis, "Uncertainty of complex permittivity measurements by split-post dielectric resonator technique," *J. Eur. Ceram. Soc.*, vol. 21, no. 15, pp. 2673–2676, Jan. 2001.
- [14] J. Krupka, "Precise measurements of the complex permittivity of dielectric materials at microwave frequencies," *Mater. Chem. Phys.*, vol. 79, no. 2–3, pp. 195–198, Apr. 2003.
- [15] J. Krupka, W. Gwarek, N. Kwietniewski, and J. G. Hartnett, "Measurements of Planar Metal–Dielectric Structures Using Split-Post Dielectric Resonators," *IEEE Trans. Microw. Theory Tech.*, vol. 58, no. 12 PART 1, pp. 3511–3518, Dec. 2010.
- [16] "PCBWay.com." [Online]. Available: <https://www.pcbway.com/>.
- [17] A. Sain and K. L. Melde, "Impact of Ground via Placement in Grounded Coplanar Waveguide Interconnects," *IEEE Trans. Compon., Packag. Manuf. Technol.*, vol. 6, no. 1, pp. 136–144,

# Supporting Information

## Estimation of the FR4 Microwave Dielectric Properties at Cryogenic Temperature for Quantum-Chip-Interface PCBs Design

A. Paghi<sup>1</sup>, G. Trupiano<sup>1</sup>, C. Puglia<sup>1,2</sup>, H. Burgaud<sup>1,3</sup>, G. De Simoni<sup>1</sup>, A. Greco<sup>1</sup>, and F. Giazotto<sup>1</sup>

<sup>1</sup> Istituto Nanoscienze-CNR and Scuola Normale Superiore, Piazza San Silvestro 12, 56127 Pisa, Italy.

<sup>2</sup> INFN Sezione di Pisa, Largo Bruno Pontecorvo 3, I-56127 Pisa, Italy.

<sup>3</sup> Ecole Normale Supérieure, 45 rue d'Ulm, 75005 Paris, France.

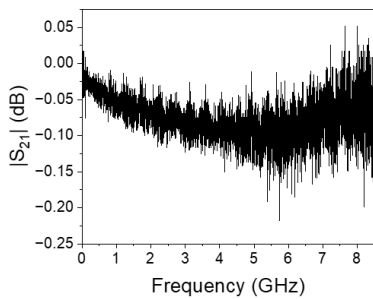


Fig. S1.  $|S_{21}|$  spectrum of the reference through at 300 K.

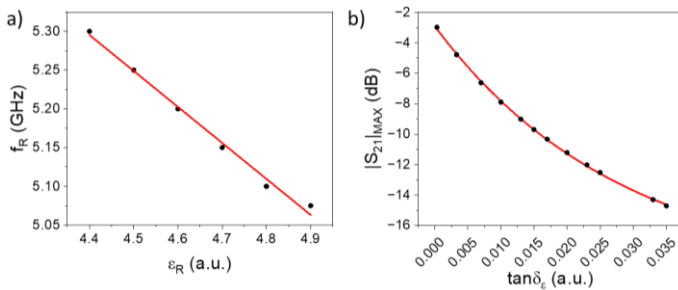


Fig. S2. a) Resonance frequency vs. real part of dielectric permittivity behaviour extrapolated from simulated spectra. The red line is the best linear fitting. b) Resonance peak magnitude vs. dielectric loss tangent behaviour extrapolated from simulated spectra. The red line is the best first order exponential decay fitting.